Experimental study on vibrating fluidized bed solids drying

Chemical Engineering Journal 472 (2023) 144809

Contents lists available at ScienceDirect

Chemical Engineering Journal

journal homepage: www.elsevier.com/locate/cej

Experimental study on vibrating fluidized bed solids drying

M.J.A. de Munck, E.A.J.F. Peters *, J.A.M. Kuipers

Multiphase Reactors Group, Department of Chemical Engineering and Chemistry, Eindhoven University of Technology, P.O. Box 513, 5600 MB Eindhoven, The Netherlands

ARTICLE INFO

Dataset link: http://dx.doi.org/10.4121/c461c907-d51a-4886-87e0-88bc08680c3b

Keywords:
Vibrating fluidized bed drying
Particle image velocimetry
Infrared thermography
Particle temperature distribution
Solids volume fluxes

ABSTRACT

Enhancing the gas–solid contacting inside a fluidized bed leads to improved solids drying characteristics. This can be achieved by mechanical vibration, resulting in so-called vibro-fluidized beds. In this study, experiments in a pseudo-2D vibro-fluidized bed setup are performed in order to better understand this improved drying behavior. A coupled particle image velocimetry - infrared thermography technique is applied to characterize the local solids velocity and temperature fields. The added vibration results in a significantly increased solids drying rate compared to a traditional gas-fluidized bed due to enhanced meso-scale particle agitation. Furthermore, it is shown that the gas-bubble appearance and the particle temperature standard deviation are highly dependent on the applied vibration amplitude and frequency.

1. Introduction

Industrial-scale solids drying is often carried out in gas-fluidized beds. Fluidized beds have excellent solids mixing characteristics as well as high volumetric gas-particle heat and mass transfer rates. These features are desired as drying is typically very energy-intensive due to the high latent heat of vaporization [1]. However, in a drying process, the gas–solid fluidized bed contacting mechanisms are very complex. The bed hydrodynamics are highly dependent on the solids mass reduction caused by the liquid evaporation, while in return, the evaporation is strongly connected to the local bed hydrodynamics [2]. Sub-optimal solids drying will therefore automatically give rise to less favorable heat and mass transfer rates. This could result in changing and unforeseen process behavior that could eventually even lead to product degradation in food or pharmaceutical applications [3,4].

By enhancing the gas–solid contacting and thus the fluidization quality, the drying mechanisms will be improved. This can be achieved by mechanical vibration, resulting in so-called vibro-fluidized beds. In the literature, it is shown that mechanical vibration can drastically improve the gas–solid fluidized bed contacting mechanisms [5–7]. Besides, mechanical vibration stabilizes the system and leads to better control of the bed dynamics [8].

Various studies have been conducted in order to obtain a better understanding of vibro-fluidization. Mawatari et al. [9] observed experimentally that the addition of mechanical vibration reduces the minimum fluidization velocity for Geldart A and C particles. More recently, McLaren et al. [10] showed similar behavior for Geldart B and D particles. Vibration also has a positive effect on bed homogeneity according to Jin et al. [11]. In the literature, mechanical vibration is characterized by a dimensionless vibration acceleration Γ which is defined as the ratio of vibration acceleration and the gravitational acceleration, g_z. The vibration acceleration depends on the vibration frequency, f_z, and amplitude, A_z:

$$\Gamma = \frac{\left(2\pi f_z\right)^2 A_z}{g_z} \tag{1}$$

Mawatari et al. [12] studied the effect of this dimensionless vibration acceleration and they showed that the descending solids flow was enhanced when the dimensionless vibrational acceleration was increased beyond a certain threshold value. Zeilstra et al. [13] employed Particle Image Velocimetry (PIV) and found that the solids circulation rate increases upon increasing the dimensionless vibrational acceleration. The effect of vibration on single gas-bubble behavior was studied in detail by Cano-Pleite et al. [14]. They reported a height-dependent phase delay between the bubble characteristics and the bed vessel displacement that is caused by compression-expansion waves traveling through the bed. The existence of the compression-expansion waves was confirmed on basis of Two-Fluid Model simulations [15]. Subsequently, the effect of vibration on the bed hydrodynamics was studied by Cano-Pleite et al. [8,16,17]. During a vibration period, the bed is expanding and compressed. Cano-Pleite et al. [17] showed that the gas-bubble expansion is dependent on the axial position. In the bottom region, the bubble expansion occurs mainly horizontally as solids penetrate the bubble through the wake, while in the top section, the bubble is expanding in both the horizontal as vertical direction.

* Corresponding author.
E-mail address: e.a.j.f.peters@tue.nl (E.A.J.F. Peters).

https://doi.org/10.1016/j.cej.2023.144809
Received 7 March 2023; Received in revised form 5 July 2023; Accepted 12 July 2023
Available online 17 July 2023

Nomenclature

A_z	Vibration amplitude (m)
d_{bed}	Depth fluidized bed (m)
f_z	Vibration frequency (Hz)
g_z	Gravitational acceleration (m/s^2)
h_{bed}	Height fluidized bed (m)
n	Number of 16 × 16 pixel windows (–)
T	Temperature (°C)
u_0	Superficial gas velocity (m/s)
u_{mb}	Minimum bubbling velocity (m/s)
u_{mf}	Minimum fluidization velocity (m/s)
w_{bed}	Width fluidized bed (m)
$\boldsymbol{\phi}$	Solids volume flux (m^3/(m^2 s))
Γ	Dimensionless vibration magnitude (–)
σ	Standard deviation particle temperature (°C)
ε_p	Solids fraction field (–)
DIA	Digital image analysis
IRT	Infrared thermography
IR	Infrared
PIV	Particle image velocimetry
PMMA	Polymethyl methacrylate

The improved bed hydrodynamics directly influence the gas–solid heat and mass transfer rates. Lehmann et al. [18] pointed out that mechanical vibration enhances the drying kinetics due to the increase of available transfer surface or the increase in transfer coefficients. Perazzini et al. [19], Stakić and Urošević [20] and Meili et al. [21] also reported improved drying rates when mechanical vibration was applied. In order to obtain a better understanding of the interplay between the improved bed hydrodynamics and the solids drying by applying mechanical vibration, more detailed information is required on the local hydrodynamics and local bed temperature.

Therefore, in this work, the detailed gas–solid interactions in vibro-fluidized beds are studied using a combined Particle Image Velocimetry (PIV) and Infra-Red Thermography (IRT) technique. This technique provides desired detailed local hydrodynamic and thermal information by converting both data sets into valuable data using a Digital Image Analysis (DIA) technique. The combined PIV/DIA technique was initially developed by van Buijtenen et al. [22] and De Jong et al. [23]. The infrared technique integration towards PIV/DIA/IR was reported by Patil et al. [24], building on the work of Tsuji et al. [25] who studied heat transfer in gas-fluidized beds. The combined technique was further extended and used for reactive systems [26], liquid injection [27–30] and for temperature distributions in a fluidized bed [31]. Recently, we employed this approach for studying drying in a conventional gas-fluidized bed [2,32].

This paper is organized as follows. In the next section, the experimental method for determining the solids velocity and temperature fields by means of the PIV/DIA/IR method is described. The results for drying monodisperse solids in a vibrating pseudo-2D fluidized bed are presented in three ways in Section 3. In the first part, we will analyze the effect of vibration on fluidized bed drying by comparing it with the static fluidized case. Secondly, the effect of the dimensionless vibration acceleration is discussed. Finally, the effect of the different used amplitudes and frequencies is analyzed. A general conclusion of this work is given in Section 4.

2. Experimental method

The vibro-fluidization experiments were carried out in a pseudo-2D fluidized bed with width 8 cm, height 20 cm and depth 1.5 cm.

Table 1
Vibration parameters of the performed experiments. The dimensionless vibration acceleration, Γ, is calculated via Eq. (1).

Γ	f_z (Hz)	A_z (mm)	Γ	f_z (Hz)	A_z (mm)
0	0	0	1	6.57	5.75
0.5	3.3	11.4	1	9.3	2.87
0.5	4.65	5.75	1.5	5.72	11.4
0.5	6.3	3.13	1.5	6.3	9.39
0.5	9.3	1.43	1.5	8.05	5.75
1	4.66	11.4	1.5	9.3	4.3
1	6.3	6.26			

The bottom of the fluidized bed consists of a porous gas-distributor plate with an average pore size equal to 10 μm where nitrogen gas was uniformly fed through. The nitrogen gas was heated using a Watlow FLUENT in-line heater. The back and side walls were made of polymethylmethacrylate (PMMA) with a thickness of 20 mm. PMMA has isolating properties due to the very low thermal conductivity that limits heat loss to the environment. The front wall is made of sapphire glass with a thickness of 3 mm. Sapphire glass has high transmittance to infrared light needed for IR measurements. The mechanical vibration is created by a LinMot H01-48 × 250/120-GF linear motor. For more detailed information on the setup, see [2,31].

2.1. Experimental procedure

Porous spherical γ-Al_2O_3 particles provided by Sasol with a size of 1.88 mm and a (dry) solids density equal to 970 kg/m^3 were used during the vibro-fluidization experiments. The dry solids mass was measured and the particles were placed in a water bath. Subsequently, the particles were put in an oven for a short time to remove the liquid layer around the outer particle surface. Subsequently, the material was cooled in the open air to a temperature of 23 °C. Afterwards, the particle weight was again measured and the water mass inside the porous particles could be determined. Finally, it was put inside a pre-heated fluidized bed setup using a gas inlet temperature of 78 °C. In the experiments, the superficial gas velocity was set to a value equal to 0.783 m/s. This gas velocity is above the obtained (dry solids) minimum fluidization velocity equal to 0.64 m/s [32].

Three different dimensionless acceleration values were studied using the vibration parameters shown in Table 1. Besides, an experiment without vertical vibration was carried out in order to directly compare the influence of vibration on a drying process.

2.2. Data acquisition

The local solids velocity and bed temperature were obtained using a high-speed optical camera PCO (Dimax HD, resolution 1080 × 720) and a high-speed infrared (IR) camera (FLIR x8400sc, resolution 1024 × 648). The optical camera was placed perpendicular to the fluidized bed and the IR camera was positioned at a slight angle with respect to the optical camera. For optimized visual image contrast, the setup was illuminated with two LED light sources. Both cameras were connected to a trigger (Velleman PCGU 1000), to control the frame rate of both cameras. The measurements were conducted with an acquisition frequency of 10 Hz.

Milacic et al. [31] and Li et al. [26] explained in detail the processing steps for the static fluidized bed case. However, the mechanical vibration resulted in a changed position of the region of interest for both cameras. Therefore, an additional processing step was added in order to correct the vertical translation caused by the mechanical vibration and this automatically resulted in the relative system of reference. In Fig. 1, a graphical example of the additional processing step is shown. The vertical translation was determined via the four stickers placed on the sides of the bed. Based on this vertical translation, all visual and infrared images were translated and cropped. Subsequently,

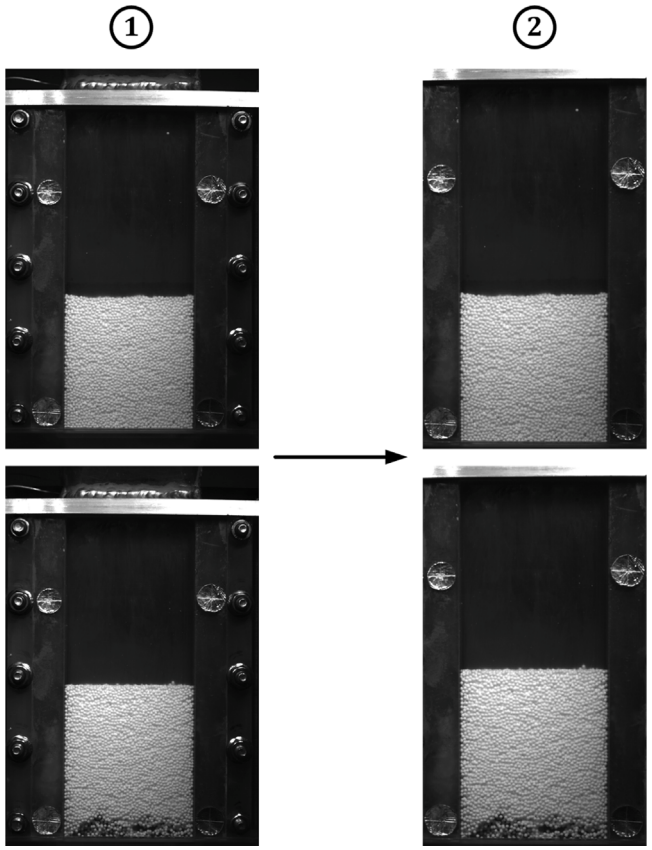

Fig. 1. Graphical example of the additional processing step required in the vibro-fluidized bed cases. The two optical images were recorded. A vertical translation needed to be carried out. Based on the four sticker locations, the vertical translation was calculated and corrected for. Besides, the image was cropped to ensure a region of interest at exactly the same position in both images (shown in step 2). Subsequently, the well-documented procedure described by Milacic et al. [31] and Li et al. [26] was carried out.

the well-documented procedure described by Milacic et al. [31] and Li et al. [26] was carried out.

The PIV processing was performed according to the method described by van Buijtenen et al. [22] and De Jong et al. [23] by using DaVis (LaVision) 8.2.3 software. See [23] for more information about the measurement uncertainties associated with PIV. PIV [33] is a non-invasive technique based on the comparison of two consecutive images taken by the optical camera, where in our case, a delay of 3.4 ms was used. An interrogation region of 64 × 64 pixels was utilized and a multi-pass algorithm with 32 × 32 pixels and 50% overlap was applied. This resulted in n 16 × 16 pixel windows, each containing a velocity vector.

Subsequently, the 3D solids volume fraction field was obtained using the method of De Jong et al. [23]. Utilizing this method, the 2D solids volume fraction was converted via a correlation to a 3D solids volume fraction field. Combining the 3D solids volume fraction field and the obtained velocity vectors results in the instantaneous solids volume fluxes calculated via:

$$\boldsymbol{\phi}(t,n) = \mathbf{v}_p(t,n)\varepsilon_p(t,n) \tag{2}$$

The infrared images were combined with the 3D solids fraction field, which led to the local solids temperature. See [24,26] for more information about the infrared temperature calibration method and the associated measurement uncertainties. By correcting for the local solids volume fraction, the instantaneous spatial average temperature was calculated according to:

$$\overline{T}_p = \frac{\sum_n \varepsilon_p(n) T_p(n)}{\sum_n \varepsilon_p(n)} \tag{3}$$

And the instantaneous particle temperature standard deviation was calculated as:

$$\sigma = \sqrt{\frac{\sum_n \varepsilon_p(n)\left(T(n) - \overline{T}_p\right)^2}{\sum_n \varepsilon_p(n)}} \tag{4}$$

3. Results and discussion

3.1. Discussion of relevant phenomena

The effect of mechanical vibration on fluidized bed drying is studied in this work. First, we present a short discussion about the effects of mechanical vibration on solids drying. This discussion is presented in order to facilitate a detailed understanding of the obtained results. In a fluidized bed, the gas–solid contacting and solids mixing have an important effect on solids drying. Both phenomena are dependent on the ratio of the superficial to minimum fluidization velocity (u_0/u_{mf}). Increasing this ratio results in larger gas bubbles due to an increased bubble coalescence rate. The gas bypassing via the bubble phase decreases the gas–solid contacting efficiency. On the other hand, larger gas bubbles enhance solids mixing. During a drying process, the bed mass is decreasing and the u_0/u_{mf} ratio increases. As a consequence, larger bubbles gradually start to appear during the process [2]. This results in less efficient gas–solid contacting but in more vigorous solids mixing.

In fluidized bed drying, the solids mixing is important since this determines the heat and mass transfer rates and the available time wherein a particle of interest is in contact with unsaturated and hot gas. Increasing the u_0/u_{mf} ratio results in more evenly distributed contact over all particles present in the bed which results in more homogeneous solids drying. Besides, more vigorous mixing also homogenizes the bed temperature since energy from hot particles is more rapidly transferred to cold solids. However, it should be noted that a larger gas volumetric flow rate results in a longer time required to fully saturate the injected gas. This increases the time wherein a particle of interest is in contact with unsaturated and hot gas. On the other hand, at low u_0/u_{mf} ratios, bed mixing is a relatively slow process due to the absence of large gas bubbles since the superficial gas velocity is close to the minimum fluidization velocity. Thus, particles located in the bottom region have a relatively large contact time with hot injected gas.

Mechanical vibration has a positive effect on both the gas–solid contacting and solids mixing. Vibration is able to compress appearing bubbles and this results in a more homogeneous state [6,11]. As mentioned, this is preferential since less gas is bypassing the solids via the bubble phase. The solids mixing is also improved by the additional force that mechanical vibration applies on the bed [13]. During the vibration sine period, defined by the vibration frequency, the vibration acceleration will temporarily improve this bed mixing. Hence, the vibration reduces the contact time with hot and unsaturated gas. This improvement is more pronounced when the superficial gas velocity is close to the minimum fluidization velocity. By changing the vibration period, the time between these applied forces differs. The vibration acceleration and thus the solids mixing degree is also dependent on the vibration amplitude. Therefore, it is expected that varying the vibration amplitude or frequency and thus the dimensionless vibrational acceleration, Γ, will result in changing gas–solid contacting, solids mixing and drying characteristics.

In order to capture these changing bed dynamics under the influence of vibration, vibrating fluidized bed drying is characterized in three ways in this work. In the first part, we will analyze the effect of vibration on fluidized bed drying by comparing it with the conventional fluidized case. Secondly, the effect of the vibration acceleration (captured by the dimensionless acceleration Γ, see Eq. (1)) is discussed. In the last subsection, the effect of different amplitudes and frequencies is analyzed. The used amount of dry porous γ-Al_2O_3 particles, the liquid content and the initial column outlet temperature are presented in Table 2. The initial column outlet temperature is noted just before the start of an experiment after preheating the empty column according to the described experimental procedure.

Table 2
Initial column temperature and the used amount of dry and wet solids material for each experiment. The amount of solids material results in a packed bed aspect ratio of one.

Experiment Γ, f_z (Hz), A_z (mm)	Initial column outlet temperature (°C)	Mass dry material (g)	Mass wet material (g)
0, 0, 0	62.0	53.53	86.55
0.5, 3.3, 11.4	61.8	53.15	85.52
0.5, 4.65, 5.75	61.4	53.23	85.52
0.5, 6.3, 3.13	61.4	52.92	87.73
0.5, 9.3, 1.43	60.4	52.70	86.91
1, 4.66, 11.4	60.4	52.42	84.59
1, 6.3, 6.26	60.0	53.42	85.69
1, 6.57, 5.75	60.1	52.91	84.50
1, 9.3, 2.87	60.9	53.11	84.90
1.5, 5.72, 11.4	61.2	53.46	85.76
1.5, 6.3, 9.39	61.6	52.58	85.60
1.5, 8.05, 5.75	60.0	52.66	83.77
1.5, 9.3, 4.3	61.0	53.05	85.34

3.2. Effect of vibration

The effect of vibration is visually presented in Figs. 2–3, showing respectively the static and the vibrating (Γ = 0.5, A_z = 5.75 mm, f_z = 4.65 Hz) fluidized bed cases. A clear difference between both experiments is observed as the static fluidized bed case resulted in a fixed bed. Similar to our previous research [2], the increased particle mass due to the addition of water inside the porous γ-Al_2O_3 resulted in a minimum fluidization velocity value above the applied superficial gas velocity. Hot air is injected into the column via the porous plate located at the bottom. As a consequence, drying proceeds via a propagating front that is dependent on the gas moisture saturation. Initially (see Fig. 2A), the whole bed is in an externally limited drying regime (i.e. wet-bulb regime). At a certain point in time, the intra-particle mass transfer becomes limiting for the solids located in the bottom region. At that point in time, the drying rate is internally limited and the energy required for the evaporation becomes less due to the reduced evaporation rate. Therefore, still some energy is left to heat up the solids. This results in large temperature differences. Due to the evaporation of liquid, the solids mass reduction leads to a lower required minimum fluidization velocity. At 510 s, this hot bed region is brought into motion by the gas–solid interaction and at 600 s, this triggers a bed inversion of hot particles originally located in the bottom region that start to move upwards (see Fig. 2C). This results in a partially fixed and fluidized bed as observed in Fig. 2D.

On the contrary, the vibro-fluidization case shows improved drying behavior. The applied superficial velocity is still lower than the required minimum fluidization velocity for the wet material. However, the added vibrational forces result in solids motion. As a consequence, the heat and mass transfer characteristics are severely improved. Therefore, a very homogeneous bed temperature is noticed during the entire experiment compared to the static fluidized bed case as seen in Fig. 3. Please note, identical temperature color bars between Figs. 2 and 3 were applied in order to show the drastically improved drying characteristics.

In order to give more details about the influence of vibration on the solids drying, the particle temperature standard deviation over time is presented in Fig. 4. As previously explained, the characteristics of the fixed-bed result in a propagating heat front, which indicates the internally limited drying regime. This results in a very large increase in the particle temperature standard deviation over time. At 510 s, this hot bed region is brought into motion by the gas–solid interaction which leads to a small decrease in the particle temperature standard deviation. After the bed inversion, the particle temperature standard deviation drastically drops due to the fluidizing motion of the dried (and hot) material. This motion results in more extensive mixing and improved heat and mass transfer characteristics. The energy from the hot solids is quickly transferred to the cold solids. Hence, the bed temperature homogenizes, indicated by the particle temperature standard deviation. On the other hand, the vibro-fluidization case shows a very small particle temperature standard deviation over the complete experiment. Therefore, it can be concluded that vibration has a positive effect on fluidized bed solids drying and temperature control when a superficial velocity close to the minimum fluidization velocity is applied.

3.3. Effect of vibration amplitude

In the previous subsection, a dimensionless vibration acceleration, Γ, equal to 0.5 already shows positive effects on the drying characteristics. It is therefore interesting to understand the effect of the vibration acceleration on the drying behavior. The experiments Γ = 0.5, A_z = 3.13 mm, f_z = 6.3 Hz, Γ = 1, A_z = 6.26 mm, f_z = 6.3 Hz and Γ = 1.5, A_z = 9.39 mm, f_z = 6.3 Hz are compared in this analysis. Fig. 5 shows visual images taken at 120 and 750 s. At, both, 120 and 750 s, the bed is in motion due to the added vibration forces. However, subtle differences in the drying process are observed. At 120 s (Fig. 5A, C E), gas-bubble formation is not observed in all three cases. McLaren et al. [10] showed that vibro-fluidization reduces the minimum required fluidization velocity more than the minimum bubbling velocity. This means that bubbles either will not be formed or fully compressed due to the bed motion as a result of the vibration. As a consequence of the drying process, the solids mass is reduced, leading to a lower required minimum fluidization and minimum bubbling velocity. Hence, the fluidization regime changes and larger bubbles start to appear. The applied vibration acceleration has a clear influence on these appearing bubbles as shown in Fig. 5B, D and F. In the lowest applied amplitude, bubbles appear, while the other two cases do not show bubble formation. This could be explained by bubble compression which is related to the applied vibration frequency and amplitude. In the case of a bubble size smaller than the bed displacement during a vibration period, no bubbles will be formed. On the other hand, a relatively small bed displacement will only lead to partial bubble compression. The vibration frequency also plays an important role, which will be discussed in detail in Section 3.4. In fluidized beds, the bubble frequency is typically in the range of 3–5 Hz. Vibration frequencies lower than the bubble frequency will result in appearing bubbles, while frequencies above the bubble frequency result in complete bubble compression. The decrease in bubble volume fraction with increasing vibration intensity was also observed by Lehmann et al. [6]. They explained that this has a positive influence on the overall drying rate. In the $\Gamma = 0.5$ case, the gas would bypass the solids via the bubble phase, while due to the increased vibration force, gas is forced to pass through the emulsion phase. This improves the gas-particle heat and mass transfer significantly.

In order to characterize these improved gas–solid contacting mechanisms, we performed an additional measurement using the vibration parameters equal to Γ = 1.5, A_z = 9.39 mm, f_z = 6.3 Hz. Due to camera data storage limitations, only a small part of the total experiment is captured when using a high, 50 Hz, acquisition frequency. This acquisition frequency allows us to capture the vibration period in more detail. Fig. 6 shows the vessel displacement created by the mechanical vibration indicated by the absolute time (750–750.30 s) and relative time of the vibration cycle. Fig. 7 shows the instantaneous solids fluxes for one vibration period in the relative system of reference. The pseudo-2D fluidized bed setup is relatively small and the column depth-to-particle size ratio is low. Therefore, it is expected that wall friction effects are more dominant than in 3D fluidized beds [34]. This could influence the obtained instantaneous solids volume fluxes. The vessel vibration results in periodic behavior of the solids motion with a phase delay compared to the vessel displacement. The observed periodic behavior follows the oscillation frequency of the vessel. The bed starts to move downwards at 750.06 s and at 750.12 s, the solids volume fluxes are evidently decreased in the bottom region as the bed comes into contact with the bottom plate. After 750.12 s, the bed

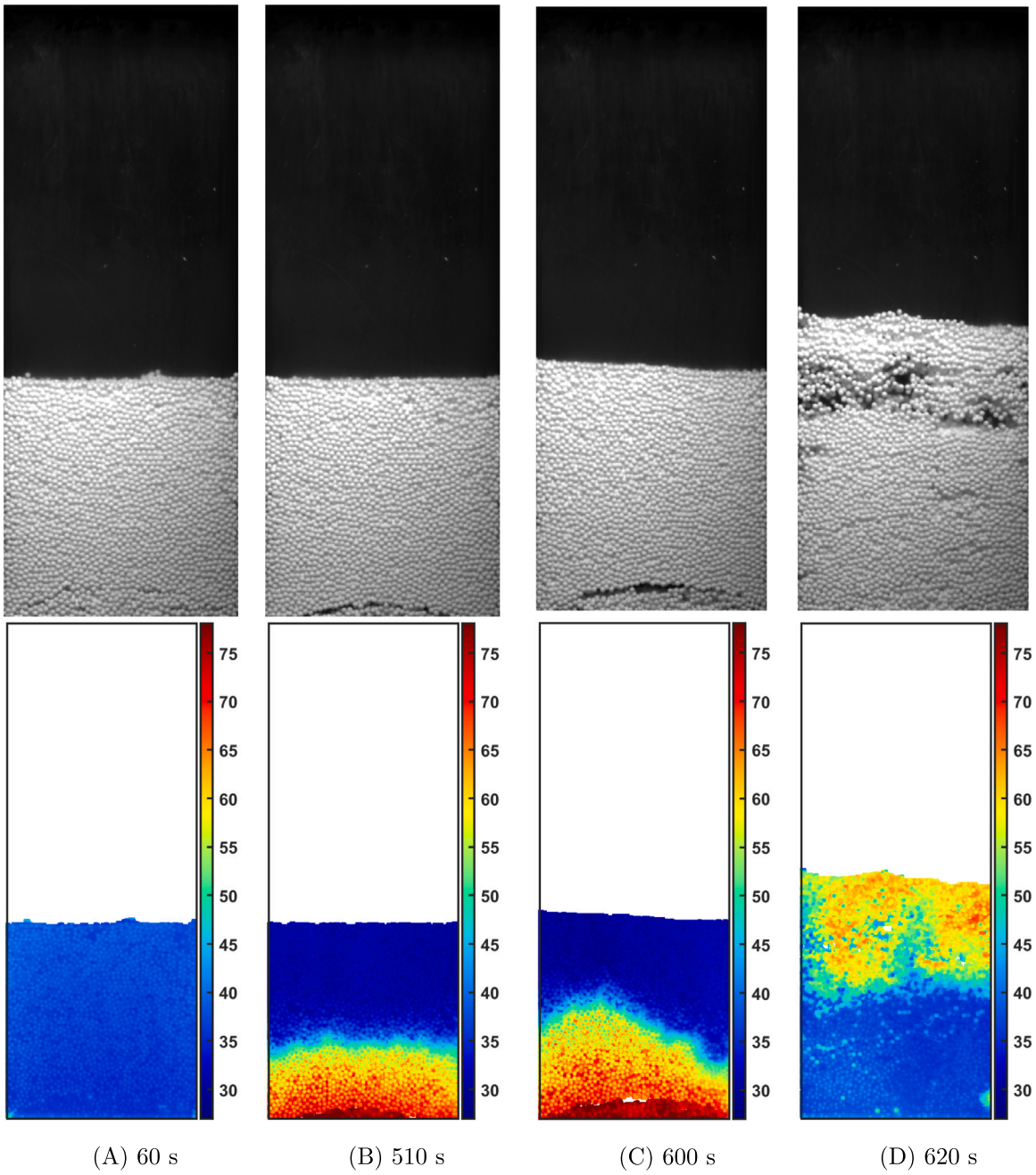

Fig. 2. Visual (top) and infrared (bottom) snapshots for the static fluidized bed case. The color bars are given in degree Celsius. The liquid content caused a particle mass increase leading to a superficial velocity lower than the required minimum fluidization velocity. Hence, the fixed bed drying front proceeds from the bottom where the hot gas is injected to the top of the bed. At 510 s, the hot (and less dense) solids are brought into motion by the gas–solid interaction and this ultimately results in a bed inversion starting at 600 s. Thereafter, the bottom part of the bed is still in a fixed state while the top section is fluidizing.

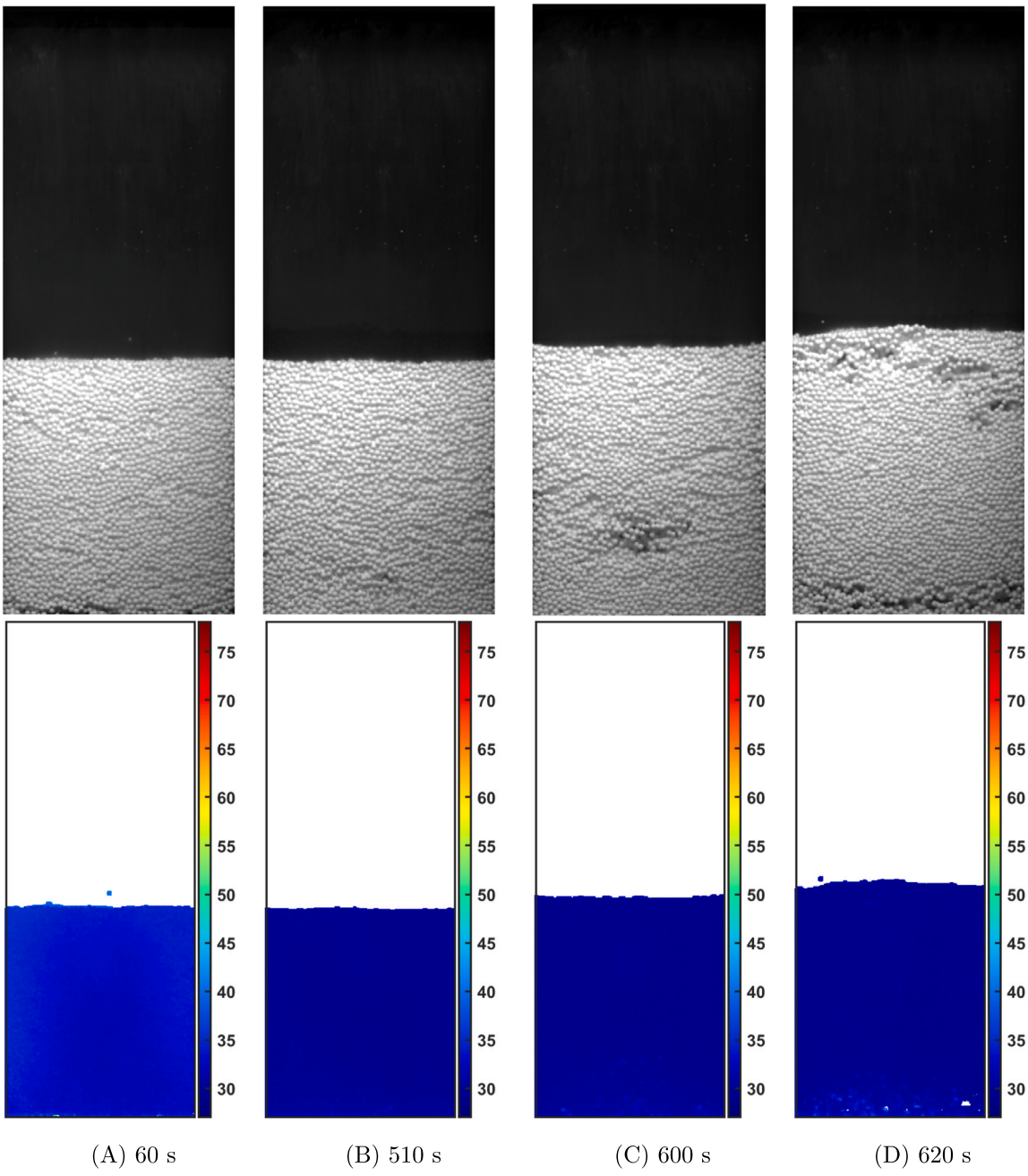

Fig. 3. Visual (top) and infrared (bottom) snapshots for the vibrating fluidized bed case (Γ = 0.5, f_z = 4.65 Hz and A_z = 5.75 mm). The color bars are given in degree Celsius. The added vibrational motion results in a mixing bed. This severely improves the drying characteristics and as a consequence, the solids dry more homogeneously compared to the static fluidized bed case.

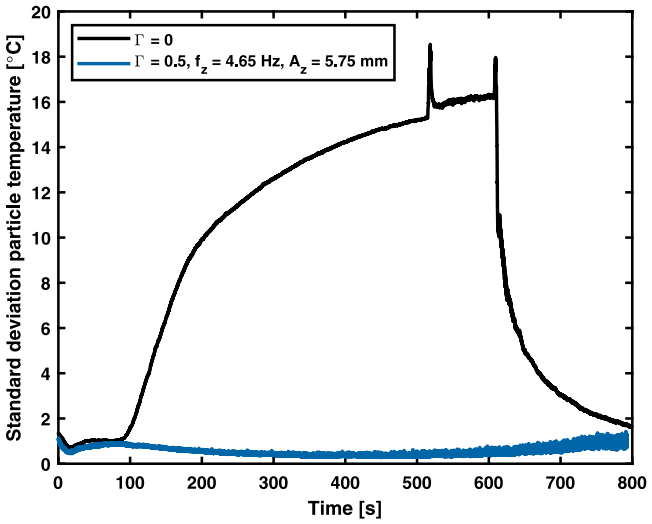

Fig. 4. Standard deviation of the particle temperature over time for the static and vibrating fluidized bed case. Vibro-fluidized bed drying drastically improves the solids drying characteristics.

motion is reversed. At 750.22 s, it reached a similar bed configuration as observed in 7A. This periodic behavior implies that in this case, the solids motion is mainly controlled by the vibration and not by the gas flow. This has a positive effect on the solids located in the wall region since the gas flow normally leads to better gas–solid contacting in the middle region of the bed due to the preferred gas bubble pathways, while the wall regions are generally seen as more stagnant regions.

The effect of the vibration cycle on the solids drying is shown in Fig. 8. During the upward bed motion, the bottom region is completely filled with hot and unsaturated gas. This unsaturated gas comes into contact with the solids during the down-going motion of the bed that starts at 750.06 s. This excess of gas is not fully saturated after contact with the bottom-located solids, hence the additional energy that is left is used to heat up the solids material. The temperature of the solids residing in the bottom region becomes higher since the bottom-located solids are in the internally limited drying regime. After 750.12 s, the solids motion is starting to reverse as the column vibration pushes the material in an upward direction. During this transition period, the bed is temporarily in a stagnant form as also observed in the solids volume fluxes shown in Fig. 7C. This results in temporary heat and mass transfer characteristics that are dominated by the gas–solid forces and not by the vibration forces. Besides, the solids volume fluxes are clearly reduced and this results in temporary fixed bed heat and mass transfer characteristics. Therefore, the temperature difference between the bottom-located solids and other sections of the bed becomes slightly higher as seen in Fig. 8D. Due to the upward motion, the bed temperature homogenizes and the vibration periodic cycle is repeated.

The periodic bed temperature change is quantified in more detail in Fig. 9A where the mean and standard deviation of the particle temperature is presented between 750 and 751.5 s. It becomes clear that a phase delay between the mean and standard deviation is present. This can be better explained by Fig. 9B showing in more detail the periodic cycle corresponding with the snapshot data presented in Fig. 8. During the upward motion, the solids temperature homogenizes, resulting in a drop of the particle temperature standard deviation. During the down-going motion of the bed that starts at 750.06 s, gas in the empty bottom region heats up the solids material, resulting in an increase of the particle temperature standard deviation, reaching a maximum at 750.8 s. Due to the high gas–solid heat transfer characteristics, the standard deviation is reduced by the energy transfer of the hot solids to other parts of the bed. After 750.12 s, the solids motion is reversed as the column vibration pushes the material in an upward motion. During this transition, the bed is temporarily in a stagnant form, resulting in an increase of the particle temperature standard deviation, reaching a maximum at 750.16 s. Thereafter, the bed motion is increased which improves the heat transfer characteristics leading to a reduction of both the particle mean and standard deviation, both reaching a minimum at 750.20 s. The mean temperature also drops due to the enhanced rate of liquid evaporation.

The vibration amplitude also changes this periodic behavior in the original experiments ($\Gamma = 0.5$, $A_z = 3.13$ mm, $f_z = 6.3$ Hz, $\Gamma = 1$, $A_z = 6.26$ mm, $f_z = 6.3$ Hz and $\Gamma = 1.5$, $A_z = 9.39$ mm, $f_z = 6.3$ Hz). It should be noted that the used acquisition frequency of 10 Hz is not high enough to capture one vibration period in more detail. Fig. 10 reveals that the increase in amplitude results in larger differences between the temporal particle temperature standard deviation. Besides it should be noted that the local temporal average value of the standard deviation is higher for the larger applied amplitude as can be seen in Fig. 10C. This can be explained by the fact that the bed temperature does not homogenize completely before the new vibration period starts.

Fig. 10 also shows a changing standard deviation over the full experiment and initially, a sharp decrease is observed. After 100 s, a decreasing trend is observed while at the end of the experiment, again an increasing temperature standard deviation is measured. The initial sharp decrease and increase till 100 s are related to the continuously changing wall temperatures that have a larger influence on the solids located near the walls. During the wet-bulb regime, the bed homogenizes where-after the solids material slowly starts to heat up again due to the transition towards the internally limited drying regime. During the internally limited drying regime, the particle temperature standard deviation is increased. Compared to the static fluidized bed case, it can be concluded that the discussed vibration experiments result in a drastically reduced particle temperature standard deviation.

3.4. Effect of vibration frequency

Another option for an increasing dimensionless vibration acceleration, Γ, is employing a higher applied vibration frequency. Therefore, the experiments $\Gamma = 0.5$, $A_z = 11.4$ mm, $f_z = 3.3$ Hz, $\Gamma = 1$, $A_z = 11.4$ mm, $f_z = 4.66$ Hz and $\Gamma = 1.5$, $A_z = 11.4$ mm, $f_z = 5.72$ Hz are compared in this analysis. Similar to Fig. 5, bubbles are not formed or fully compressed at the start of all three experiments. At the end of the experiments, similar differences between the dimensionless vibrational acceleration values of 0.5, 1 and 1.5 cases are found. Bubbles are formed in the Γ equal to 0.5 case. On the other hand, no bubbles are observed in the 1.0 and 1.5 dimensionless acceleration cases. This follows the explanation from the previous discussion regarding the applied vibration frequency and amplitude compared to the bubble frequency and size.

The drying behavior as a function of the vibration acceleration is captured in Fig. 11. Initially, a sharp decrease is observed followed by an increasing standard deviation. After 100 s, a decreasing trend is observed while at the end of the experiment clear differences are found between Fig. 11A, B and C. At the end of the experiment, the drying is internally limited and this causes a temperature increase of the solids material. In the case of a well-mixed system, this temperature increase is quickly homogenized over the full bed. However, this is not the case in the $\Gamma = 0.5$, $A_z = 11.4$ mm, $f_z = 3.3$ Hz experiment. This can be better understood via snapshots presented in Fig. 12. It shows similar but less pronounced behavior as in the static fluidized bed (i.e. without vibration) as hot and less dense solids material in the bottom zone starts to move upwards whereafter the hot solids temperature is reduced due to the heat transfer with the surrounding relative cold gas and particles. This means that this vibration amplitude and frequency combination is not able to fully homogenize the bed temperature. The reason is the relatively low applied vibration frequency that results in a large vibration period and as a consequence, the solids mixing is too low. See

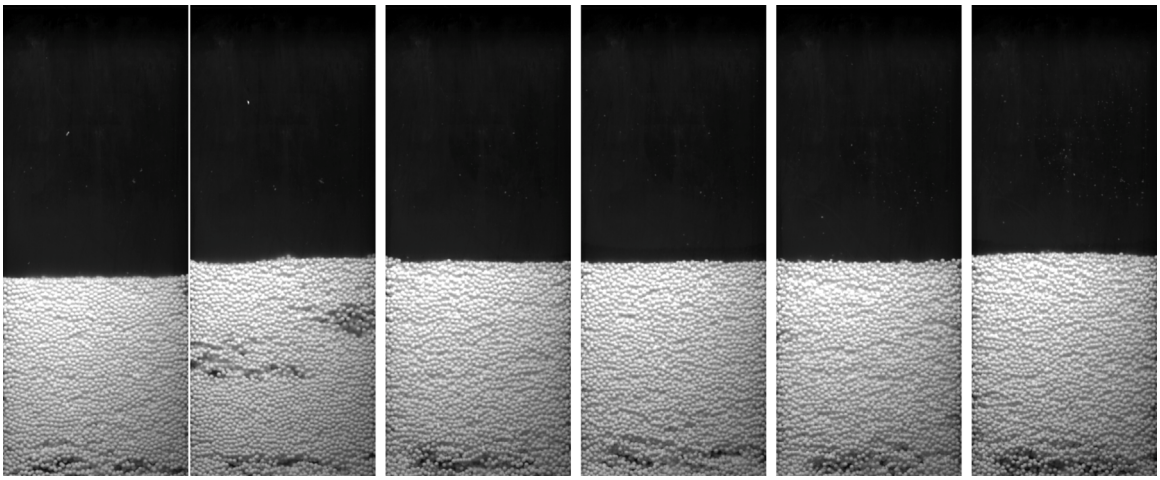

Fig. 5. Visual images of the Γ = 0.5, A_z = 3.13 mm, f_z = 6.3 Hz, Γ = 1, A_z = 6.26 mm, f_z = 6.3 Hz and Γ = 1.5, A_z = 9.39 mm, f_z = 6.3 Hz cases for 120 and 750 s. The bed is in a downgoing motion in all snapshots. In (B), gas bubbles are formed and by increasing the vibration acceleration, bubbles are not observed in (D) and (F).

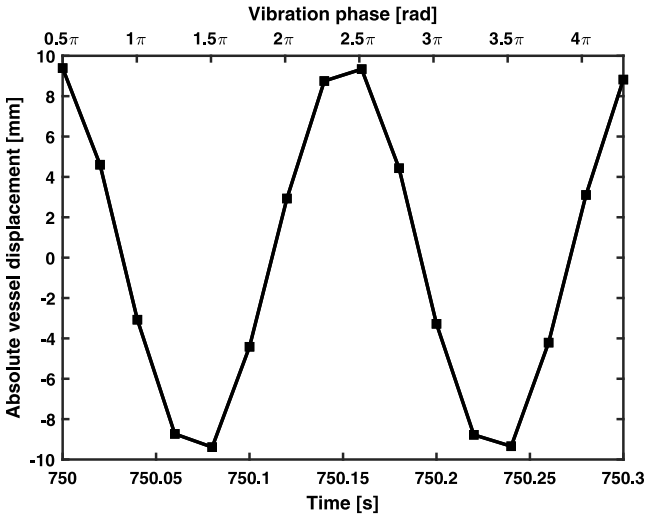

Fig. 6. Vessel displacement created by the mechanical vibration indicated by the absolute time and relative time of the vibration cycle for the Γ = 1.5, A_z = 9.39 mm, f_z = 6.3 Hz experiment.

the next subsection for a detailed discussion about this effect. Therefore, the gas-particle contact time of material located in the bottom zone is too large, leading to larger temperature differences. However, it should be noted that the temperature differences are smaller compared to the static fluidized bed case where a very large particle temperature standard deviation was obtained.

3.5. Effect of amplitude and frequency

Various vibration amplitude–frequency combinations could lead to exactly the same dimensionless vibration acceleration Γ. Daleffe et al. [35] and Meili et al. [21,36] explained that this ratio should be chosen with care. In this analysis, we first examine the bed hydrodynamic behavior of the dimensionless vibrational acceleration equal to 0.5. Similar to the previous discussion, initially gas bubbles were not formed or fully compressed while at the end of the experiment, in all cases bubbles were detected as shown in Fig. 13 at 750 s. This bubble formation was observed in all combinations since the bubble frequency and/or the diameter is higher than the applied vibration amplitude and frequency.

Similar to Daleffe et al. [35] and Meili et al. [21,36], we also found that the drying behavior is not similar for the four cases we tested using a Γ value equal to 0.5. Fig. 14 shows the particle temperature standard deviation for the different experiments. It is observed that a larger applied amplitude results in larger differences between the temporal solids temperature distribution. In the previous subsection, we discussed the large increase of the particle temperature standard deviation shown in Fig. 14D. Therefore, very different drying behavior is encountered for a constant dimensionless Γ value calculated in Eq. (1).

This can be explained by the sine acceleration curve where the behavior between the maximum and minimum acceleration values is not taken into account. For the Γ = 0.5, A_z = 11.4 mm, f_z = 3.3 Hz and Γ = 0.5, A_z = 1.43, f_z = 9.3 Hz cases, both amplitude–frequency combinations lead to the desired maximum applied acceleration equal to 4.905 m/s^2 (i.e. Γ = 0.5). However, the vibration periodic time is different and this causes the changed fluidization behavior. In vibro-fluidized beds, the bed hydrodynamics will be determined by the ratio of the applied gas–solid and the vibration forces. At the point in time where the maximum vibration acceleration is applied, the vibration force is more dominant compared to the point in time where the vibration acceleration is almost equal to zero due to the transition from the upward to downward vibration motion. Therefore, it means that the applied vibration acceleration needs a certain threshold to dominate over the gas–solid forces in order to impact the bed hydrodynamics. However, in the f_z = 3.3 Hz case, the time where the vibration acceleration does not dominate the bed hydrodynamics is larger than for the f_z = 9.3 Hz. In order words, both the vibration and gas–solid forces are dominating for a longer consecutive period in the f_z = 3.3 Hz case compared to the f_z = 9.3 Hz case. Since the gas–solid forces result in inferior solids mixing due to the applied superficial velocity which is close to the minimum fluidization velocity, the temperature of the bottom-located solids starts to rise, resulting in a larger temperature difference inside the bed.

In the Γ equal to 1.5 cases, also differences regarding the hydrodynamic behavior were found. In Fig. 15A and B, small bubbles appeared that were not fully suppressed by the used vibration amplitude and frequency combination. On the other hand, Fig. 15C and D show no appearing gas bubbles since both the frequency and amplitude are larger than respectively the bubble frequency and size. However, the Γ equal to 1.5 cases do not result in very different drying characteristics compared to the Γ equal to 0.5 cases. The main reason is that the vibration forces are larger and also dominate the gas forces over a larger part of the vibration period.

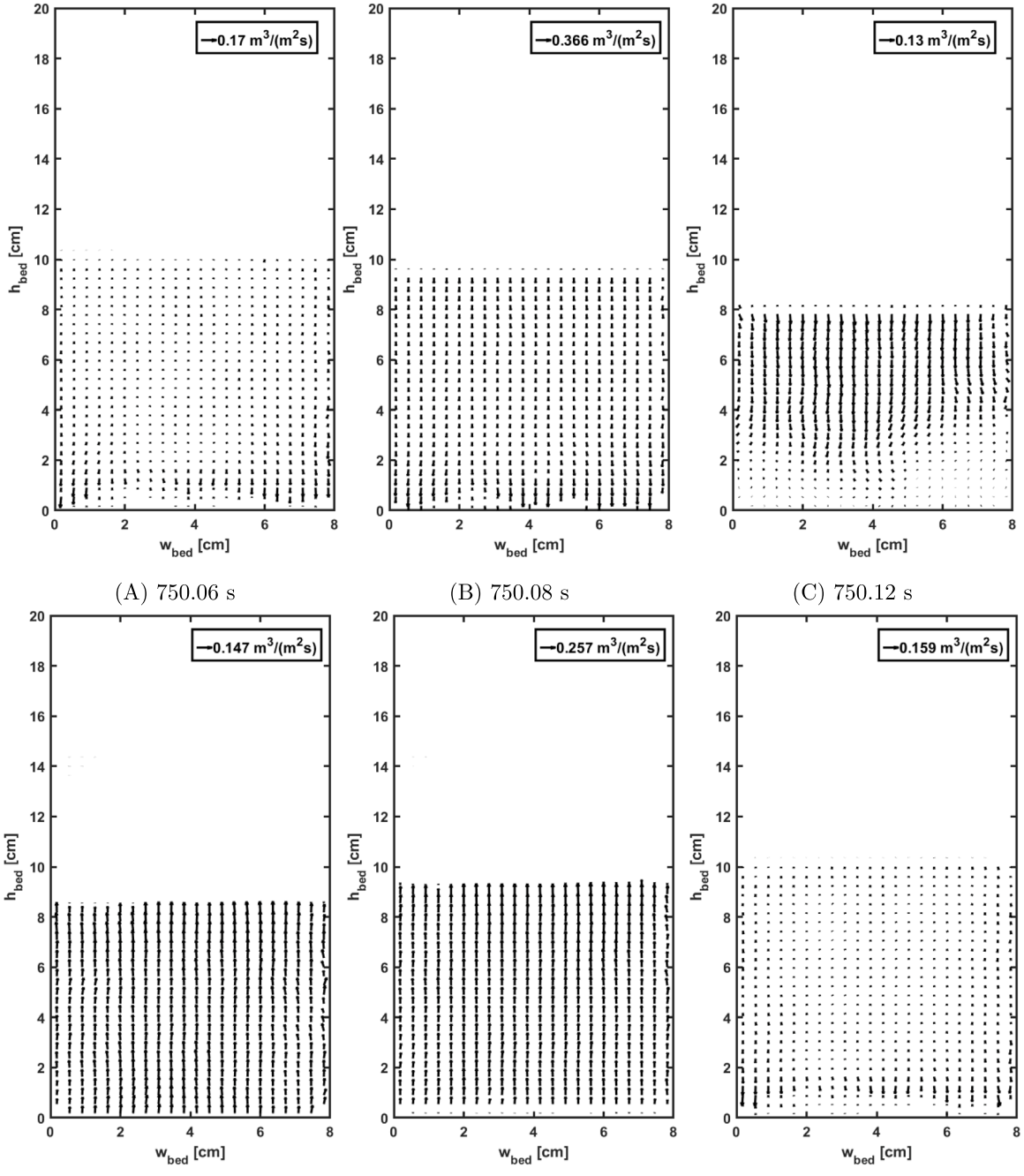

(A) 750.06 s (B) 750.08 s (C) 750.12 s

(D) 750.16 s (E) 750.18 s (F) 750.22 s

Fig. 7. Instantaneous solids volume fluxes during one vibration period using Γ = 1.5, A_z = 9.39 mm, f_z = 6.3 Hz. Please note the scale differences.

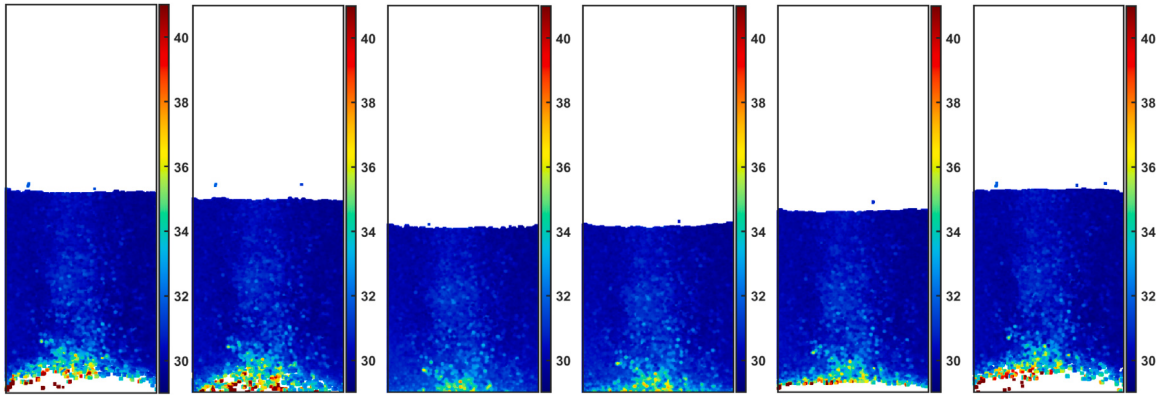

(A) 750.06 s (B) 750.08 s (C) 750.12 s (D) 750.16 s (E) 750.18 s (F) 750.22 s

Fig. 8. Snapshots of the bed temperature for the vibrating fluidized bed case $\Gamma = 1.5$, $A_z = 9.39$ mm, $f_z = 6.3$ Hz over one vibration cycle. The color bars are given in degree Celsius. During the downward bed motion, the bottom-located solids temperature increases. Between (C) and (D), the solids motion is reversed, resulting in temporarily fixed bed heat and mass transfer characteristics. In the upward motion, the bed temperature quickly homogenizes.

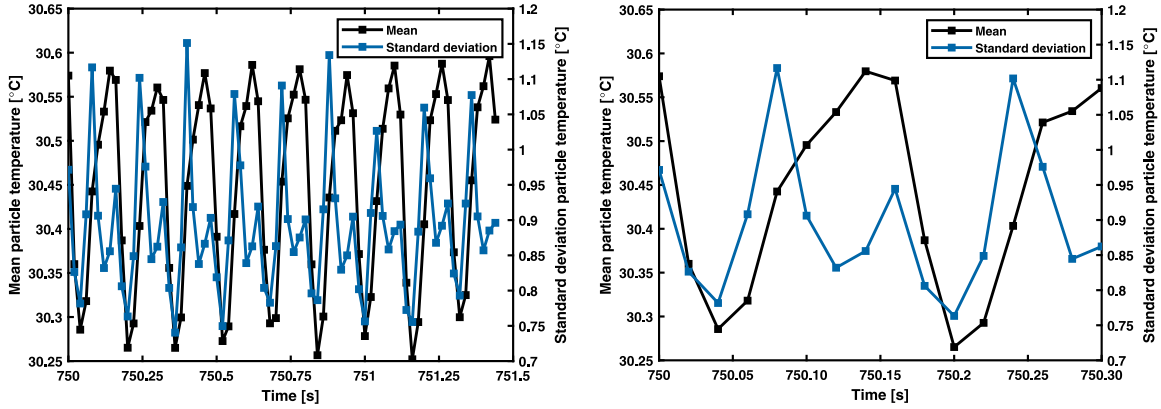

(A) Periodic trend 750-751.5 s (B) Periodic trend 750-750.30 s

Fig. 9. Mean and standard deviation particle temperature for the additional $\Gamma = 1.5$, $A_z = 9.39$ mm, $f_z = 6.3$ Hz experiment using an acquisition frequency equal to 50 Hz. A clear periodic trend is observed which corresponds with the applied vibration frequency. The used vibration amplitude is causing the fluctuating temperature values.

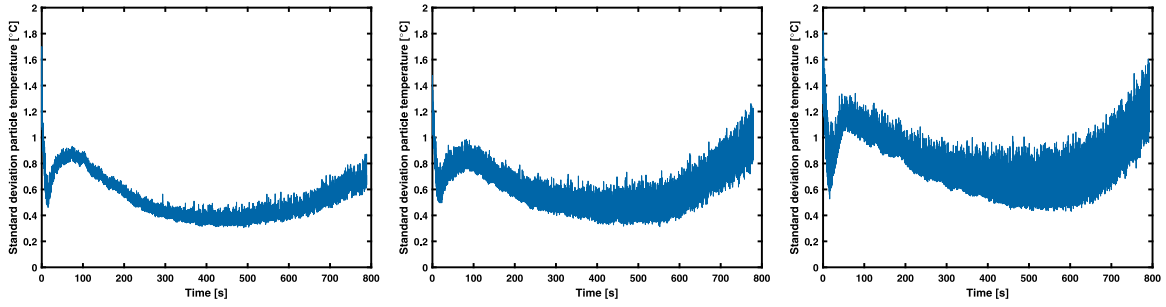

(A) $\Gamma = 0.5$ (B) $\Gamma = 1$ (C) $\Gamma = 1.5$

Fig. 10. Particle temperature standard deviation over the full experiments ($\Gamma = 0.5$, $A_z = 3.13$ mm, $f_z = 6.3$ Hz, $\Gamma = 1$, $A_z = 6.26$ mm, $f_z = 6.3$ Hz and $\Gamma = 1.5$, $A_z = 9.39$ mm, $f_z = 6.3$ Hz). The increased amplitude causes larger differences between the temporal particle temperature standard deviation.

4. Conclusions

Monodisperse porous γ-Al_2O_3 particles were dried in a pseudo-2D vibro-fluidized bed setup. A combined PIV and IRT technique was employed to study the local particle hydrodynamic behavior and the particle temperature. It is observed that the addition of vibration severely improved the solid drying characteristics. The static fluidized bed experiment resulted in a fixed bed with the corresponding less favorable heat and mass transfer rates, while vibro-fluidization case showed drastically improved drying features which were quantified using the particle temperature standard deviation.

The effect of the vibration acceleration was studied over Γ values equal to 0.5, 1.0 and 1.5. It becomes clear that bubble formation in vibro-fluidized beds is dependent on the reducing solids density. The solids density reduction causes a changing fluidizing behavior due to the shifted ratio between the superficial to minimum fluidization velocity. In the case of more vigorous fluidization, larger bubbles will appear. It was found that gas bubbles will be compressed in the case

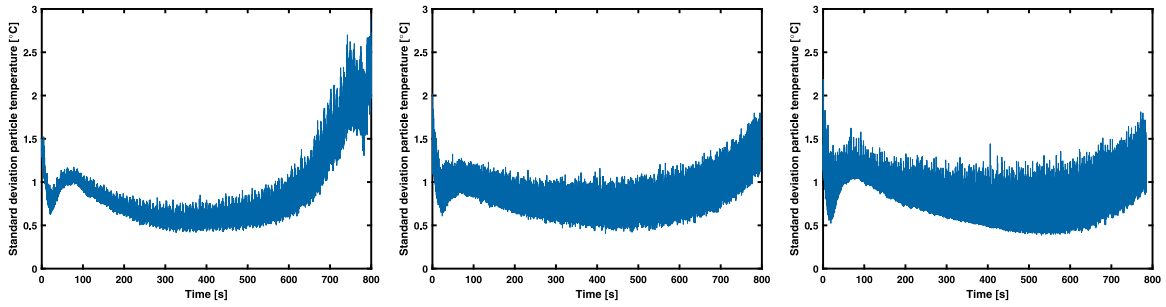

Fig. 11. Particle temperature standard deviation over the full experiments (Γ = 0.5, A_z = 11.4 mm, f_z = 3.3 Hz, Γ = 1, A_z = 11.4 mm, f_z = 4.66 Hz and Γ = 1.5, A_z = 11.4 mm, f_z = 5.72 Hz). The applied frequency and amplitude in (A) result in relatively low solids mixing. Therefore, the gas-particle contact time of material located in the bottom zone is too large, leading to larger temperature differences.

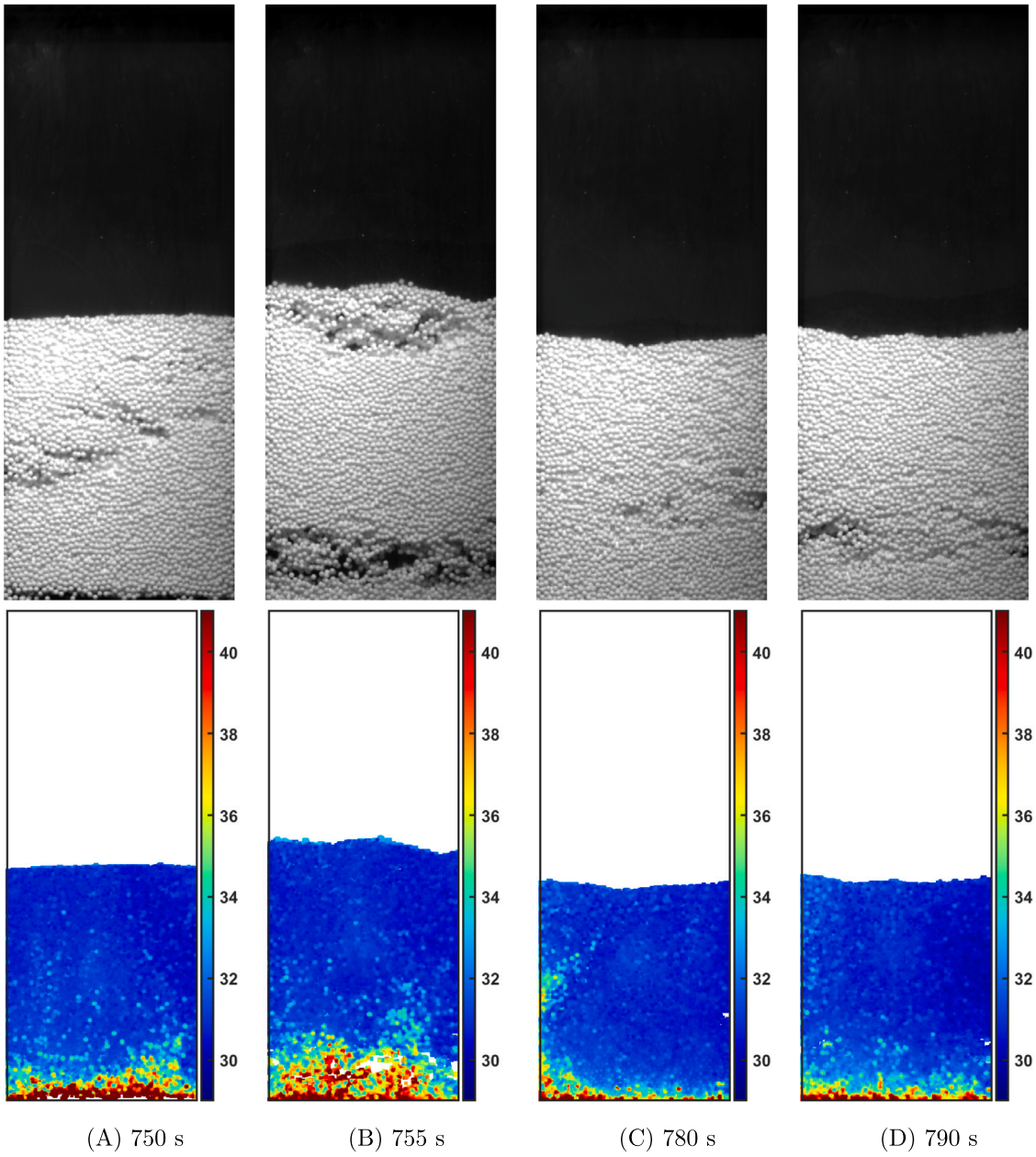

Fig. 12. Visual (top) and infrared (bottom) snapshots for the Γ = 0.5, A_z = 11.4 mm, f_z = 3.3 Hz case. The color bars are given in degree Celsius. The applied frequency and amplitude in (A) result in relatively low solids mixing. Therefore, the gas-particle contact time of material located in the bottom zone is too large, leading to larger temperature differences. Hot and less dense solids move upwards whereafter the hot solids temperature is reduced due to the heat transfer with the surrounding relative cold gas and particles.

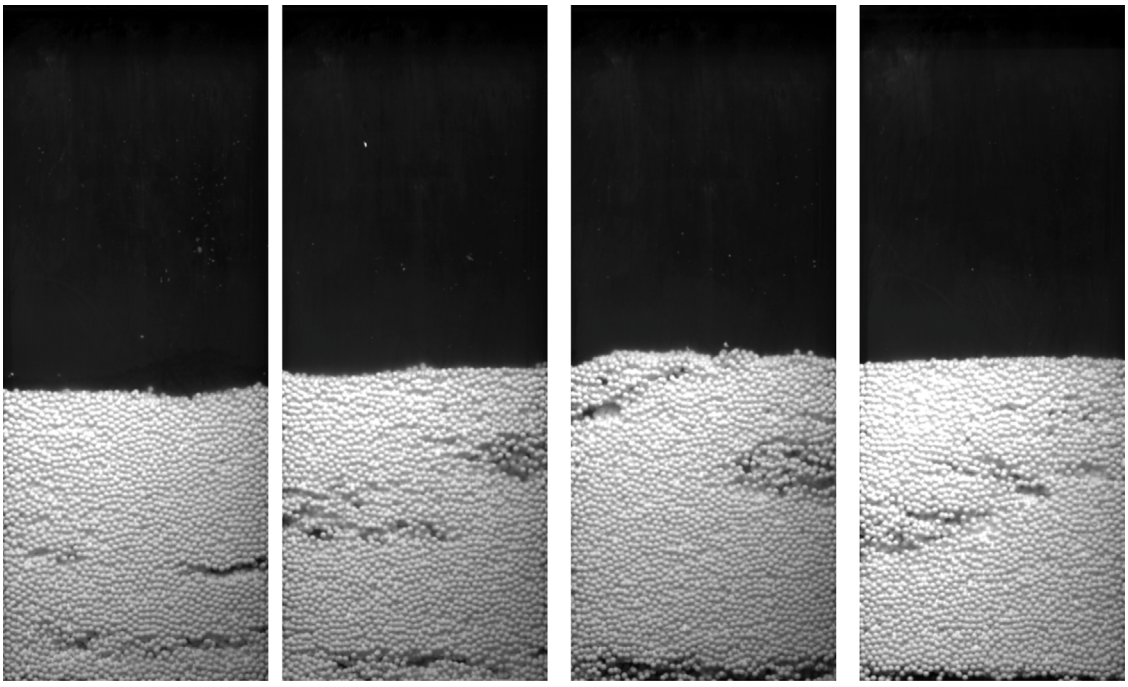

(A) $A_z = 1.43$ mm, $f_z = 9.3$ Hz (B) $A_z = 3.13$ mm, $f_z = 6.3$ Hz (C) $A_z = 5.75$ mm, $f_z = 4.65$ Hz (D) $A_z = 11.4$ mm, $f_z = 3.3$ Hz

Fig. 13. Snapshots of the Γ = 0.5 cases taken at 750 s. Bubble formation is observed in all cases as either or both the bubble frequency or diameter is higher than the applied vibration amplitude and frequency.

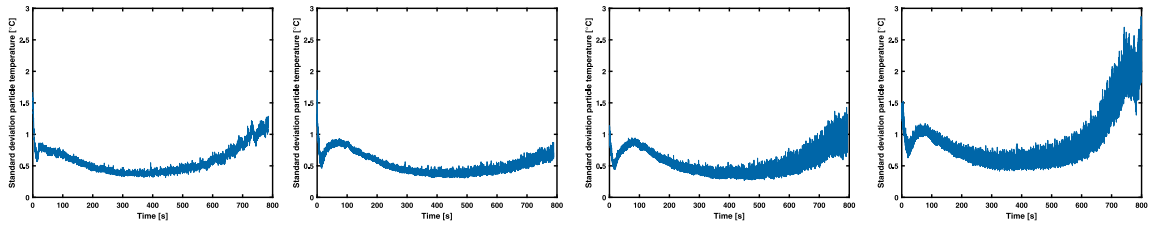

(A) $A_z = 1.43$ mm, $f_z = 9.3$ Hz(B) $A_z = 3.13$ mm, $f_z = 6.3$ Hz (C) $A_z = 5.75$ mm, $f_z = 4.65$ Hz (D) $A_z = 11.4$ mm, $f_z = 3.3$ Hz

Fig. 14. Particle temperature standard deviation over the full experiment for the Γ equal to 0.5 cases. An increasing vibration amplitude results in larger differences between the temporal standard deviation.

where the vibration frequency is larger than the bubble frequency in combination with an applied vibration amplitude larger than the bubble size. Therefore, this bubble compression is dependent on the u_0/u_{mf} ratio and the chosen vibration amplitude and frequency. An experiment applying an acquisition frequency of 50 Hz showed in more detail the periodic effect of the vibration on the bed temperature. It was observed that the temporal change in the particle temperature standard deviation follows the vibration period.

The effect of the applied amplitude and frequency ratio revealed different bed hydrodynamics even within a constant applied dimensionless vibration acceleration Γ. This resulted in changing solids drying characteristics whereof some combinations demonstrated unfavorable bed behavior. This could be explained by the periodic sine wave that is used in mechanical vibration. During the sine wave period, the ratio between the gas-solids and vibration forces is changing. At the point in time that the gas-solids forces are too weak to establish sufficient solids mixing, the solids drying becomes more inhomogeneous at the point in time where the applied vibration forces become low. In the case of a low vibration acceleration established by a high amplitude (and thus a low frequency), a substantial time in between the dominance of the vibration forces results in a relatively long contact time with the hot injected gas. In higher vibration acceleration cases, this effect was not observed since the vibration forces are larger and dominate the gas–solid forces over a larger part of the vibration period.

Declaration of competing interest

The authors declare that they have no known competing financial interests or personal relationships that could have appeared to influence the work reported in this paper.

Data availability

A data package is available at the 4TU Research Data repository, DOI: http://dx.doi.org/10.4121/c461c907-d51a-4886-87e0-88bc08680c3b.

Acknowledgments

This research received funding from the Dutch Research Council (NWO) in the framework of the ENW PPP Fund for the top sectors and from the Ministry of Economic Affairs in the framework of the "PPS-toeslagregeling". We would like to thank Marlieke Breijer-Pepels, Hans

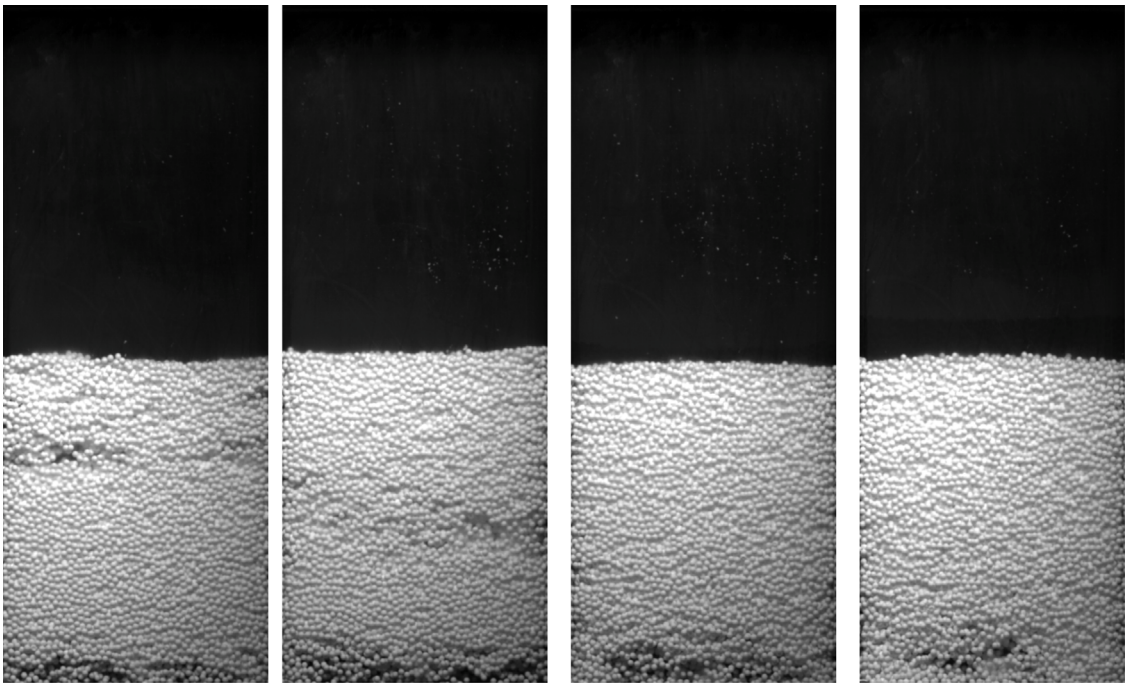

(A) $A_z = 4.3$ mm, $f_z = 9.3$ Hz (B) $A_z = 5.75$ mm, $f_z = 8.05$ Hz (C) $A_z = 9.39$ mm, $f_z = 6.3$ Hz (D) $A_z = 11.4$ mm, $f_z = 5.72$ Hz

Fig. 15. Snapshots of the $\Gamma = 1.5$ cases taken at 750 s. Bubble formation is observed in (A) and (B), while in (C) and (D) the bubble formation is fully suppressed by the applied vibration amplitude and frequency.

Meerman and Henk Jan Panneman for the fruitful discussions and Joop Aarts, Herbert Fiedler and Larry de Graaf for their valuable technical support.

References

[1] T. Defraeye, Advanced computational modelling for drying processes - A review, Appl. Energy 131 (2014) 323–344.

[2] M.J.A. De Munck, E.A.J.F. Peters, J.A.M. Kuipers, Experimental investigation of monodisperse solids drying in a gas-fluidized bed, Chem. Eng. Sci. 259 (2022) 117783.

[3] R. Sivakumar, R. Saravanan, A. Elaya Perumal, S. Iniyan, Fluidized bed drying of some agro products - A review, Renew. Sustain. Energy Rev. 61 (2016) 280–301.

[4] Y. Zhang, N. Abatzoglou, S. Hudon, P.P. Lapointe-Garant, J.S. Simard, Dynamics of heat-sensitive pharmaceutical granules dried in a horizontal fluidized bed combined with a screw conveyor, Chem. Eng. Process.: Process Intensif. (2021) 167.

[5] F. Raganati, R. Chirone, P. Ammendola, Gas-solid fluidization of cohesive powders, Chem. Eng. Res. Des. 133 (2018) 347–387.

[6] S.E. Lehmann, E.U. Hartge, A. Jongsma, I.M. DeLeeuw, F. Innings, S. Heinrich, Fluidization characteristics of cohesive powders in vibrated fluidized bed drying at low vibration frequencies, Powder Technol. 357 (2019) 54–63.

[7] V. Francia, K. Wu, M.O. Coppens, Dynamically structured fluidization: Oscillating the gas flow and other opportunities to intensify gas-solid fluidized bed operation, Chem. Eng. Process. Process Intensif. 159 (2021) 108143.

[8] E. Cano-Pleite, F. Hernández-Jiménez, A. Acosta-Iborra, Bulk oscillation and velocity wave propagation in a vibrated fluidized bed at minimum fluidization conditions, Powder Technol. 308 (2017) 346–361.

[9] Y. Mawatari, Y. Tatemoto, K. Noda, Prediction of minimum fluidization velocity for vibrated fluidized bed, Powder Technol. 131 (2003) 66–70.

[10] C.P. McLaren, J.P. Metzger, C.M. Boyce, C.R. Müller, Reduction in minimum fluidization velocity and minimum bubbling velocity in gas-solid fluidized beds due to vibration, Powder Technol. 382 (2021) 566–572.

[11] H. Jin, Z. Tong, J. Zhang, B. Zhang, Homogeneous fluidization characteristics of vibrating fluidized beds, Can. J. Chem. Eng. 82 (2004) 1048–1053.

[12] Y. Mawatari, K. Tagawa, Y. Tatemoto, K. Noda, Bubbling characteristics under vertical vibration in a two-dimensional fluidized bed, J. Chem. Eng. Japan 38 (2005) 18–23.

[13] C. Zeilstra, M.A. Van der Hoef, J.A.M. Kuipers, Experimental and numerical study of solids circulation in gas-vibro fluidized beds, Powder Technol. 248 (2013) 153–160.

[14] E. Cano-Pleite, F. Hernández-Jiménez, M. de Vega, A. Acosta-Iborra, Experimental study on the motion of isolated bubbles in a vertically vibrated fluidized bed, Chem. Eng. J. 255 (2014) 114–125.

[15] E. Cano-Pleite, F. Hernández-Jiménez, A. Acosta-Iborra, Compressible-gas two-fluid modeling of isolated bubbles in a vertically vibrated fluidized bed and comparison with experiments, Chem. Eng. J. 271 (2015) 287–299.

[16] E. Cano-Pleite, Y. Shimizu, A. Acosta-Iborra, Y. Mawatari, Effect of vertical vibration and particle size on the solids hold-up and mean bubble behavior in a pseudo-2D fluidized bed, Chem. Eng. J. 304 (2016) 384–398.

[17] E. Cano-Pleite, F. Hernández-Jiménez, A. Acosta-Iborra, Y. Mawatari, Oscillatory behavior of the bed bulk and the bubbles in a vertically vibrated pseudo-2d bed in bubbling regime, Chem. Eng. J. 312 (2017) 228–242.

[18] S.E. Lehmann, T. Oesau, A. Jongsma, F. Innings, S. Heinrich, Material specific drying kinetics in fluidized bed drying under mechanical vibration using the reaction engineering approach, Adv. Powder Technol. 31 (2020) 4699–4713.

[19] H. Perazzini, F.B. Freire, J.T. Freire, The influence of vibrational acceleration on drying kinetics in vibro-fluidized bed, Chem. Eng. Process.: Process Intensif. 118 (2017) 124–130.

[20] M. Stakić, T. Urošević, Experimental study and simulation of vibrated fluidized bed drying, Chem. Eng. Process.: Process Intensif. 50 (2011) 428–437.

[21] L. Meili, H. Perazzini, M.C. Ferreira, J.T. Freire, Analyzing the universality of the dimensionless vibrating number based on the effective moisture diffusivity and its impact on specific energy consumption, Heat Mass Transfer/Waerme-Stoffuebertrag. 56 (2020) 1659–1672.

[22] M.S. van Buijtenen, M. Börner, N.G. Deen, S. Heinrich, S. Antonyuk, J.A.M. Kuipers, An experimental study of the effect of collision properties on spout fluidized bed dynamics, Powder Technol. 206 (2011) 139–148.

[23] J.F. De Jong, S.O. Odu, M.S. Van Buijtenen, N.G. Deen, M. Van Sint Annaland, J.A.M. Kuipers, Development and validation of a novel digital image analysis method for fluidized bed particle image velocimetry, Powder Technol. 230 (2012) 193–202.

[24] A.V. Patil, E.A.J.F. Peters, V.S. Sutkar, N.G. Deen, J.A.M. Kuipers, A study of heat transfer in fluidized beds using an integrated DIA/PIV/IR technique, Chem. Eng. J. 259 (2015) 90–106.

[25] T. Tsuji, T. Miyauchi, S. Oh, T. Tanaka, Simultaneous measurement of particle motion and temperature in two-dimensional fluidized bed with heat transfer, KONA Powder Part. J. 28 (2010) 167–179.

[26] Z. Li, T.C.E. Janssen, K.A. Buist, N.G. Deen, M. van Sint Annaland, J.A.M. Kuipers, Experimental and simulation study of heat transfer in fluidized beds with heat production, Chem. Eng. J. 317 (2017) 242–257.

[27] V.S. Sutkar, N.G. Deen, A.V. Patil, E.A.J.F. Peters, J.A.M. Kuipers, V. Salikov, S. Antonyuk, S. Heinrich, Experimental study of hydrodynamics and thermal behavior of a pseudo-2d spout-fluidized bed with liquid injection, AIChE J. 61 (2015) 1146–1159.

[28] T. Kolkman, J.A.M. van Sint Annaland, Whole-field imaging of temperature and hydrodynamics in a gas fluidized bed with liquid injection, Chem. Eng. Sci. 168 (2017) 23–40.

[29] E. Milacic, M. Nunez Manzano, S. Madanikashani, G.J. Heynderickx, K.M. Van Geem, M.W. Baltussen, J.A.M. Kuipers, Liquid injection in fluidized bed: Temperature uniformity, Chem. Eng. Sci. 256 (2022) 117622.

[30] E. Milacic, D.R. Rantong, J.A.M. Kuipers, M.W. Baltussen, Temperature distribution in fluidized beds of porous particles with LiquidInjection, Chem.-Ingen.-Tech. (2022) 1–8.

[31] E. Milacic, M. Nunez Manzano, S. Madanikashani, G.J. Heynderickx, K.M. van Geem, A.A.M. van de Greef, L. Hickethier, A. Richter, S.H.L. Kriebitzsch, K.A. Buist, M.W. Baltussen, J.A.M. Kuipers, Experimental study on the temperature distribution in fluidised beds, Chem. Eng. Sci. 248 (2022) 117062.

[32] M.J.A. De Munck, M. Dullemond, E.A.J.F. Peters, J.A.M. Kuipers, Experimental gas-fluidized bed drying study on the segregation and mixing dynamics for binary and ternary solids, Chem. Eng. J. 465 (2023) 142756.

[33] J. Westerweel, Fundamentals of digital particle image velocimetry, Meas. Sci. Technol. 8 (1997) 1379–1392.

[34] T. Li, P. Gopalakrishnan, R. Garg, M. Shahnam, CFD–DEM study of effect of bed thickness for bubbling fluidized beds, Particuology 10 (2012) 532–541.

[35] R.V. Daleffe, M.C. Ferreira, J.T. Freire, Drying of pastes in vibro-fluidized beds: Effects of the amplitude and frequency of vibration, Drying Technol. 23 (2005) 1765–1781.

[36] L. Meili, R.V. Daleffe, J.T. Freire, Fluid dynamics of fluidized and vibrofluidized beds operating with Geldart C particles, Chem. Eng. Technol. 35 (2012) 1649–1656.